Preparations, Structures, and Properties of Copper(II) Complexes with a New Tripodal Tetradentate Ligand, *N*-(2-Pyridylmethyl)bis(6-pivalamido-2-pyridylmethyl)amine, and Reactivities of the Cu(I) Complex with Dioxygen

Manabu Harata, Koji Hasegawa, Koichiro Jitsukawa,* Hideki Masuda,* and Hisahiko Einaga

Department of Applied Chemistry, Nagoya Institute of Technology, Showa-ku, Nagoya 466-8555

(Received October 27, 1997)

Copper complexes of a tripodal tetradentate ligand, *N*-(2-pyridylmethyl)bis(6-pivalamido-2-pyridylmethyl)amine (Hbppa), have been prepared as a model of metal centers of mononuclear copper enzymes; their structures and properties have been examined together with those having several secondary ligands by electronic absorption, ESR and FAB mass spectral, cyclic voltammetric, and X-ray diffraction methods. The complexes, $[Cu(Hbppa)](ClO_4)_2$ and $[Cu(Hbppa)(N_3)]\cdot ClO_4\cdot H_2O$, were obtained as single crystals, whose crystal structures revealed square-planar and trigonal-bipyramidal geometries, respectively. The electronic absorption and ESR spectra for the Cu^{II}(Hbppa)–X systems (X = no, Cl^-, Br^-, I^-, N_3^-, and CH_3COO^-) allowed us to conclude that the complexes form several coordination geometries, such as square-planar, square-pyramidal, and trigonal-bipyramidal, depending upon the solvents (MeOH, MeCN). The redox potentials of [Cu(Hbppa)Cl]Cl in MeCN, THF, MeOH, and CH_2Cl_2 showed quasi-reversible Cu^I/Cu^{II} couples in the range of −0.056—+0.085 V vs. Ag/AgCl at room temperature. The addition of dioxygen to the Cu(I)–Hbppa, which was prepared from $[Cu(MeCN)_4]PF_6$ and Hbppa (1 : 1) in EtCN at −78°C, resulted in a graduate absorption spectral change with two well-separated absorption maxima at 665 ($\varepsilon = 162\ M^{-1}\,cm^{-1}$) and 837 nm ($\varepsilon = 305\ M^{-1}\,cm^{-1}$) and an intense band at 375 nm ($\varepsilon = 641\ M^{-1}\,cm^{-1}$) as a shoulder. Simultaneous ESR experiments of the same complex solution exhibited a silent spectrum, indicating that the complex is diamagnetic. A similar electronic absorption spectral change was observed in MeOH with absorption peaks at 387 nm ($\varepsilon = 843\ M^{-1}\,cm^{-1}$), 640 ($\varepsilon = 183\ M^{-1}\,cm^{-1}$) and 828 ($\varepsilon = 289\ M^{-1}\,cm^{-1}$), although the ESR spectrum did not continue to be completely silent. Increasing the temperature of the solution up to room temperature demonstrated the formation of $[Cu(Hbppa)(OH)]^-$ species, whose X-ray structure was $[Cu(Hbppa)(OH)]PF_6\cdot H_2O$. The reaction of the $[Cu(Hbppa)]ClO_4$–sodium benzoylformate system with dioxygen in DMF resulted in production of carbon dioxide and benzoic acid, as analyzed by GC and HPLC.

The metal–oxygen species occur at heme iron,[1,2] non-heme iron[3,4] and copper enzyme active centers[5—10] in biological systems. Detailed examinations of such systems are very important in understanding the biological processes, such as oxygen transport, oxidation, oxygenation, and dehydrogenation.[11] In order to elucidate the interaction modes between the metals and dioxygen, many investigations have been performed by use of appropriate ligands with low molecular weight.[11,12] However, fewer studies on copper–dioxygen systems[5—10] have been performed, in spite of the importance in biological copper oxidase systems, because of the difficulty of its experimental treatment, especially the Jahn–Teller effect in copper(II) species and the instability of copper(I) species. The difficulties may be settled by appropriate modifications of the ligands. In order to obtain more detailed understanding of the copper–oxygen interactions and reactivities, we have synthesized some mononuclear copper complexes with new tripodal tetradentate ligands: tris(6-pivalamido-2-pyridylmethyl)amine (Htppa)[13] and *N*-(5-carboxyl-2-pyridylmethyl)bis(6-pivalamido-2-pyridylmethyl)-amine (bpca).[14] The design concepts of these novel ligands are as follows: (i) four coordination sites for a metal ion, (ii) hydrogen bonding NH groups to fix a small molecule such as dioxygen in the vicinity of the metal, (iii) hydrophobic *t*-butyl groups to protect the small bound molecule and to prevent dinucleation of coordinated metal centers, and (iv) electron-withdrawing pivaloylamido groups to stabilize a lower valence state of copper.[26] Recently, we designed a tripodal tetradentate ligand, *N*-(2-pyridylmethyl)bis(6-pivalamido-2-pyridylmethyl)amine (Hbppa) (Chart 1), which gives an accessible space of substrate at the reaction center, and succeeded in the preparation of the Cu(II)–Hbppa complex with hydrogen peroxide.[15]

Here, we describe the binding ability of the Cu(II)–Hbppa complex with a small substrate and the reactivity of the Cu(I)–Hbppa complex with a dioxygen molecule. Furthermore, the oxidative cleavage reaction of α-keto acid by the superoxide activated by the Cu^I–Hbppa complex is also discussed. The ligands employed for the oxidative cleavage reaction, Htppa, Hbppa, tnpa (tris[6-(neopentylamino)-2-pyridylmethyl]amine), and bpqa (*N*-(2-quinolylmethyl)bis(6-pivalamido-2-pyridylmethyl)amine), are shown in Chart 1.

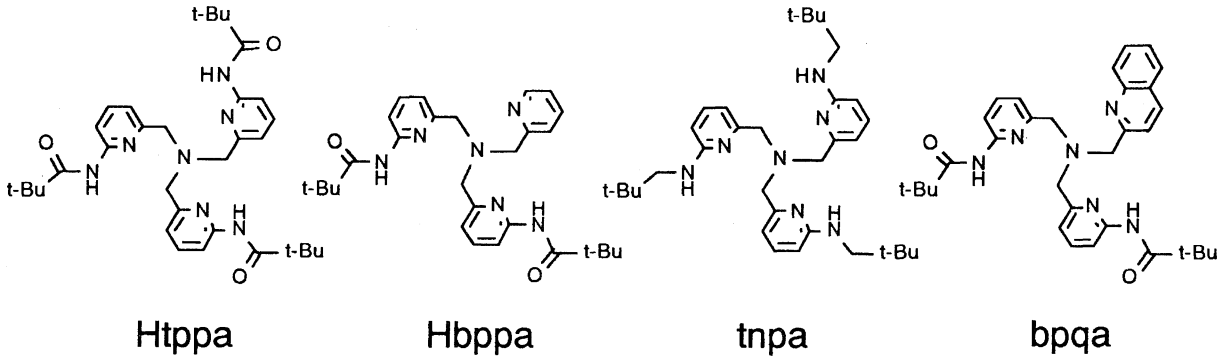

Chart 1.

Experimental

Materials and Measurements. Reagents and solvents employed were of the highest grade available. All solvents for spectroscopies were purified by further distillation before use. Other chemicals were used without further purification.

Electronic absorption spectra were measured at −78 °C on a JASCO UVIDEC-660 spectrophotometer equipped with a San-ei Giken low temperature cell. X-band ESR spectra of frozen solutions were recorded at 77 K using a JEOL RE-1X ESR spectrometer. ^{1}H NMR spectra were measured on a JEOL Lambda-500 spectrometer with TMS as an internal standard. Positive-ion FAB mass spectra were obtained with a Shimadzu Kratos Concept I S.

Cyclic voltammetric measurements were performed using a Bioanalytical Systems (BAS) CV-27 Voltammograph equipped with a Graphtec X–Y WX2400 chart recorder. A 3-mm diameter glassy-carbon working electrode, an Ag/AgCl reference electrode, and a Pt-wire counter electrode were used in a glass cell having a working compartment (approximately 10-mL in volume). All measurements were made at 25 °C under an argon atmosphere in solution with tetrabutylammonium tetrafluoroborate (0.1 M, 1 M = 1 mol dm^{-3}) as a supporting electrolyte at a scan rate of 100 mV s^{-1}.

HPLC analyses were performed with a JASCO 900 system under isocratic conditions with a flow rate of 1 mL min^{-1} using a Whatman Partisil ODS-C18 column (4.6 mmϕ × 150 mm). The UV detector for monitoring the products and reactant was set at 254 nm. Product analyses were performed using an Okura 202 system gas chromatograph equipped with a TCD detector using an active charcoal column (3 mm × 5 m).

Synthesis of Hbppa. Hbppa was synthesized from *N*-(6-methyl-2-pyridyl)pivalamide according to the following procedure (Scheme 1). The structure and purity were confirmed by ^{1}H NMR spectroscopy and X-ray structure analysis.

***N*-(6-Methyl-2-pyridyl)pivalamide.** To a CH_2Cl_2 (150 mL) solution containing 2-amino-6-methylpyridine (30.0 g, 0.28 mol) in the presence of triethylamine (36.4 g, 0.36 mol) was added pivaloyl chloride (33.8 g, 0.28 mol); the reaction solution was then stirred at room temperature for 2 h. The crude product was purified by recrystallization from ether to give *N*-(6-methyl-2-pyridyl)pivalamide (45.0 g, 83.6% yield).

***N*-[6-(Bromomethyl)-2-pyridyl]pivalamide.** To a CCl_4 solution (250 mL) of *N*-(6-methyl-2-pyridyl)pivalamide (19.2 g, 0.10 mol) was added NBS (17.8 g, 0.10 mol) and a catalytic amount of AIBN; then the solution was refluxed for 6 h at 80 °C. After cooling, the resulting mixture containing *N*-[6-(bromomethyl)-2-pyridyl]-pivalamide, 6-(dibromomethyl)-2-pyridyl compound (by-product) and unreacted *N*-(6-methyl-2-pyridyl)pivalamide was washed with a 2.5 M sodium hydrogencarbonate solution and then dried over $MgSO_4$. After the separation by evaporation in vacuo from the reaction solution, the crude oil obtained was purified by silica gel column chromatography with a hexane–AcOEt (5 : 1) mixture as an eluent to give *N*-[6-(bromomethyl)-2-pyridyl]pivalamide (11.7 g, 43.3% yield).

***N*-(2-Pyridylmethyl)bis(6-pivalamido-2-pyridylmethyl)amine (Hbppa).** Reaction of the primary amine, 2-pyridylmethylamine, (1.40 g, 13.0 mmol) with the two molar amounts of *N*-[6-(bromomethyl)-2-pyridyl]pivalamide (8.13 g, 30.0 mmol) was carried out in a dioxane/H_2O (4 : 1) solution (300 ml) containing KOH (2.92 g, 52.0 mmol). After the reaction solution was stirred at room temperature for 2 d, it was neutralized with 1 M HCl and evaporated in vacuo to yield a crude brownish oil. The recrystallization from ether gave colorless needle-like crystals of Hbppa (2.25 g, 35.5% yield). ^{1}H NMR (δ/ppm from TMS in $CDCl_3$) δ = 1.33 (s, 18H, $C(CH_3)_3$), 3.75 (s, 4H, $-CH_2-$, H6), 3.88 (s, 2H, $-CH_2-$, H1), 7.15

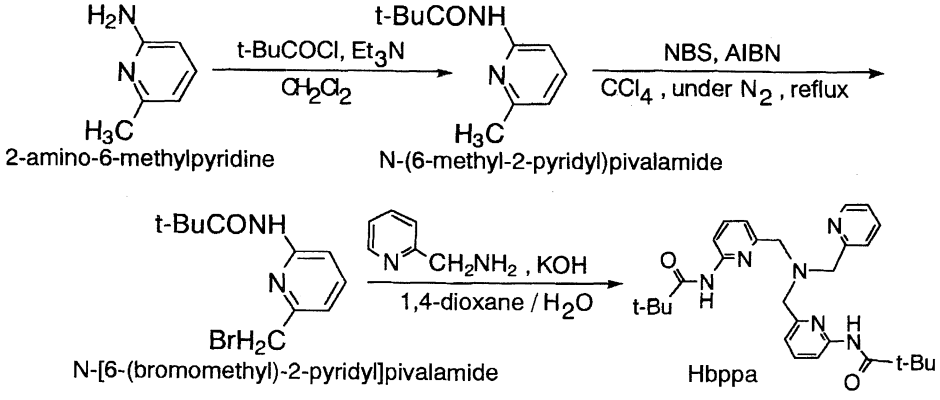

Scheme 1.

(t, 1H, H4), 7.30 (d, 2H, H7), 7.55 (d, 1H, H2), 7.65 (t, 1H, H3), 7.67 (t, 2H, H8), 7.96 (s, 2H, amide-NH), 8.11 (d, 2H, H9), 8.53 (d, 1H, H5). FAB-mass spectra: *m/z* 489 $[(C_{28}H_{36}N_6O_2)+H^+]^+$.

Syntheses of BPQA and TNPA. The preparations of BPQA[17] and TNPA[18] were performed by the methods described in the literature.

Preparation of [Cu(Hbppa)](ClO$_4$)$_2$. To a stirred MeOH solution (25 mL) of $Cu(ClO_4)_2\cdot 6H_2O$ (37.1 mg, 0.10 mmol) was added Hbppa (48.8 mg, 0.10 mmol). After the resulting mixture was allowed to stand at room temperature for a few days, blue crystals of $[Cu(Hbppa)](ClO_4)_2$ suitable for X-ray structure analysis were obtained.

Preparations of [Cu(Hbppa)(X)]$^+$ (X = Cl$^-$, Br$^-$, and I$^-$). The preparation of $[Cu(Hbppa)Cl]^+$ was carried out by the addition of KCl (32 mg, 0.43 mmol) to an MeCN solution (25 mL, 2.0 mM) of $Cu(ClO_4)_2\cdot 6H_2O$ (19.0 mg, 5.1×10^{-2} mmol) and Hbppa (26.0 mg, 5.3×10^{-2} mmol). The complex [Cu(Hbppa)Cl]Cl was recrystallized from MeCN solution. Anal. Calcd for $C_{28}H_{36}N_6O_2CuCl_2$: C, 48.95; H, 5.281; N, 12.23%. Found: C, 48.99; H, 5.096; N, 12.08%. The formation of $[Cu(Hbppa)Cl]^+$ was also confirmed by the parent peak of the positive ion FAB mass spectrum *m/z* 586 for $[C_{28}H_{36}N_6O_2CuCl]^+$.

Preparation of $[Cu(Hbppa)Br]^+$ and $[Cu(Hbppa)I]^+$ was carried out by the same method as that of $[Cu(Hbppa)Cl]^+$ below. That of $[Cu(Hbppa)Br]^+$ was performed by the addition of KBr (51 mg, 0.43 mmol) to a MeCN solution (25 mL, 2.0 mM) solution of $Cu(ClO_4)_2\cdot 6H_2O$ (19.0 mg, 5.1×10^{-2} mmol) and Hbppa (26.0 mg, 5.3×10^{-2} mmol). The preparation of $[Cu(Hbppa)I]^+$ was performed by the addition of KI (78 mg, 0.43 mmol) to an MeCN solution (25 mL, 2.0 mM) solution of $Cu(ClO_4)_2\cdot 6H_2O$ (19.0 mg, 5.1×10^{-2} mmol) and Hbppa (26.0 mg, 5.3×10^{-2} mmol). The formation of these complexes was confirmed by parent peaks of positive ion FAB mass spectrum: *m/z* 632 for $[Cu(Hbppa)Br]^+$ and 678 for $[Cu(Hbppa)I]^+$, respectively. The sample solutions prepared above were subjected to measurements of electronic absorption and ESR spectra.

Preparation of [Cu(Hbppa)(N$_3$)]ClO$_4$·H$_2$O. To an MeCN solution (5 mL, 20 mM) of $[Cu(Hbppa)](ClO_4)_2\cdot H_2O$ (86.8 mg, 0.10 mmol) was added NaN_3 (14.3 mg, 0.22 mmol). The green precipitate formed immediately was filtered off, and was recrystallized from MeCN to give 75 mg (97%) of the product. This complex, crystallized from MeCN to give plate-like green single crystals, is suitable for X-ray structure analysis on standing at room temperature.

Preparation of [Cu(bppa)]ClO$_4$. To a stirred MeOH solution (2.0 mL) of $Cu(ClO_4)_2\cdot 6H_2O$ (37.1 mg, 0.10 mmol) and Hbppa (48.8 mg, 0.10 mmol) was added KOH (5.61 mg, 0.10 mmol). After the resulting mixture was allowed to stand at room temperature, a green precipitate of $[Cu(bppa)]ClO_4$ suitable for elemental analysis and ESI-mass spectroscopy was obtained. Anal. Calcd for $C_{28}H_{35}N_6O_6CuCl$: C, 51.69; H, 5.42; N, 12.92%. Found: C, 51.78; H, 5.45; N, 12.67%. Positive ion FAB-mass spectra *m/z* 550 $[(C_{28}H_{35}N_6O_2Cu)+H^+]^+$.

Preparation of [Cu(Hbppa)(CH$_3$COO)]ClO$_4$. To a stirred MeCN solution (2.0 mL) of $Cu(CH_3COO)_2\cdot H_2O$ (20.0 mg, 0.10 mmol) and Hbppa (48.8 mg, 0.10 mmol) was added $NaClO_4$ (12.2 mg, 0.10 mmol). After the mixture was allowed to stand at room temperature for a few days, a blue precipitate of $[Cu(Hbppa)(CH_3COO)]ClO_4$ was obtained. Anal. Calcd for $C_{30}H_{39}N_6O_8CuCl$: C, 50.70; H, 5.53; N, 11.83%. Found: C, 50.73; H, 5.441; N, 11.75%.

Reaction of [Cu(Hbppa)]PF$_6$ with Dioxygen. To an EtCN solution (4 mL, 2 mM) of $[Cu(MeCN)_4]PF_6$ (2.9 mg, 7.9×10^{-3} mmol) was added Hbppa (4.2 mg, 8.6×10^{-3} mmol) at room temperature under thorough bubbling with Ar, which was employed for the reaction with dioxygen. The preparation in MeOH was performed by the same procedure as that in EtCN.

Reaction of the Cu(I)–Hbppa–Sodium Benzoylformate System with Dioxygen. To a DMF solution (4 mL) containing $[Cu(MeCN)_4]ClO_4$ (2.6 mg, 7.9×10^{-3} mmol) and Hbppa (4.2 mg, 8.6×10^{-3} mmol) was added sodium benzoylformate (1.4 mg, 8.1×10^{-3} mmol) under an Ar atmosphere at room temperature. After stirring the reaction mixture for 15 min, the yellowish reaction solution cooled at −78 °C was bubbled with O_2 gas. As the reaction proceeded, the color of the reaction solution turned blue. After the temperature of the solution was raised to room temperature and the solution was stirred for 4 h, CO_2 gas was detected by GC analysis in the reaction vessel, which indicates the decarboxylation of benzoylformate. The yield of the decarboxylated compound, benzoic acid, was determined by HPLC analysis. For comparison, the reactions were also carried out for Htppa, bpqa, and tnpa complexes (Chart 1).

X-Ray Structure Analyses of Hbppa, [Cu(Hbppa)](ClO$_4$)$_2$, [Cu(Hbppa)(N$_3$)]ClO$_4$·H$_2$O and [Cu(Hbppa)(OH)]PF$_6$·H$_2$O. Crystals of each of these compounds, suitable for X-ray diffraction measurements, were mounted on a glass capillary. The diffraction data were collected with graphite-monochromated Mo $K\alpha$ radiation on an Enraf–Nonius CAD4-EXPRESS four-circle diffractometer at room temperature with the ω–2θ scan technique. Crystal data and experimental details are listed in Table 1.

All the structures were solved by a combination of direct method and Fourier techniques, and all the non-hydrogen atoms were anisotropically refined by full-matrix least-squares calculations. Atomic scattering factors and anomalous dispersion terms were taken from the International Tables for X-ray Crystallography.[19] Empirical absorption corrections using Ψ-scans were applied for all crystals after full isotropic refinements of non-hydrogen atoms. Since the number of reflection data were not enough to refine all the parameters of the non-hydrogen and hydrogen atoms, they were not included for further refinement; their positions were determined from difference Fourier maps, except for a part of the hydrogen atoms of the water molecules. Calculations were carried out on a micro VAX 3100 computer by using the MolEN program.[20] Tables of the atomic coordinates, thermal parameters, bond lengths and angles, torsion angles, and observed and calculated structure factors have been deposited as Document No. 71024 at the Office of the Editor of Bull. Chem. Soc. Jpn.

Results and Discussion

Synthesis and Structure of Hbppa. The novel mononucleating ligand Hbppa was prepared through a multistep process summarized in Scheme 1 (also see Experimental Section), which is a synthetic method modified from that of the previous ligand Htppa.[13b] The structure of Hbppa was confirmed from FAB-mass and ^{1}H NMR spectroscopies and X-ray crystal structure analysis. As shown in Fig. 1, Hbppa is a tripodal tetradentate ligand composed of a central tertiary nitrogen, one pyridyl methyl nitrogen and the two pyridine rings which are substituted by pivalamido group.

Electronic Absorption and ESR Spectra of [Cu(Hbppa)]$^{2+}$ Complexes with Small Anions. The electronic absorption spectral data of samples obtained by re-

Table 1. Crystallographic Data and Experimental Details for Hbppa, $[Cu(Hbppa)](ClO_4)_2$, $[Cu(Hbppa)(N_3)]ClO_4 \cdot H_2O$, and $[Cu(Hbppa)(OH)]PF_6 \cdot H_2O$

	Hbppa	$[Cu(Hbppa)](ClO_4)_2$	$[Cu(Hbppa)(N_3)]ClO_4 \cdot H_2O$	$[Cu(Hbppa)(OH)]PF_6 \cdot H_2O$
Formula	$C_{28}H_{36}N_6O_2$	$C_{28}H_{36}N_6O_{10}CuCl_2$	$C_{28}H_{38}N_9O_7CuCl$	$C_{28}H_{39}N_6O_4CuPF_6$
F.W.	488.63	751.08	711.66	732.17
Color	Colorless	Blue	Green	Green
Crystal dimensions/mm	$0.3 \times 0.5 \times 0.8$	$0.3 \times 0.3 \times 0.5$	$0.3 \times 0.3 \times 0.4$	$0.3 \times 0.4 \times 0.4$
Crystal system	Monoclinic	Monoclinic	Monoclinic	Monoclinic
Space group	$P2_1/c$ (# 14)	$P2_1/c$ (# 14)	$P2_1/n$ (# 14)	$P2_1/n$ (# 14)
a/Å	10.1776(6)	12.5582(8)	13.736(2)	10.2079(5)
b/Å	9.7344(5)	17.973(2)	18.337(2)	22.555(2)
c/Å	27.990(2)	14.846(1)	14.572(1)	15.454(1)
β/deg	90.115(5)	93.056(5)	103.856(9)	106.266(5)
V/Å^3	2773.0(3)	3346.1(4)	3563.6(7)	3415.8(5)
D_{calcd}/g cm^{-3}	1.170	1.491	1.326	1.424
Z	4	4	4	4
$F(000)$	1048	1556	1484	1516
μ(Mo $K\alpha$)/cm^{-1}	0.710	8.742	7.400	7.572
Radiation	Graphite monochromated Mo $K\alpha$ ($\lambda = 0.71073$ Å)			
T/°C	21	21	21	21
$2\theta_{max}$/deg	52.64	52.64	52.64	52.64
No. of reflections measured	5096	7352	7805	7503
No. of reflections used [$I > 3.00\sigma(I)$]	2032	2730	2503	2271
No. of Variables	326	425	416	416
S	2.249	1.484	2.047	1.713
R;R_w[a)]	0.060;0.070	0.047;0.050	0.065;0.074	0.059;0.060

a) $R = \Sigma||F_o| - |F_c||/\Sigma|F_o|$. $R_w = [\Sigma w(|F_o| - |F_c|)^2/\Sigma w|F_o|^2]^{1/2}$; $w = 4F_o^2/\sigma^2(F_o)^2$.

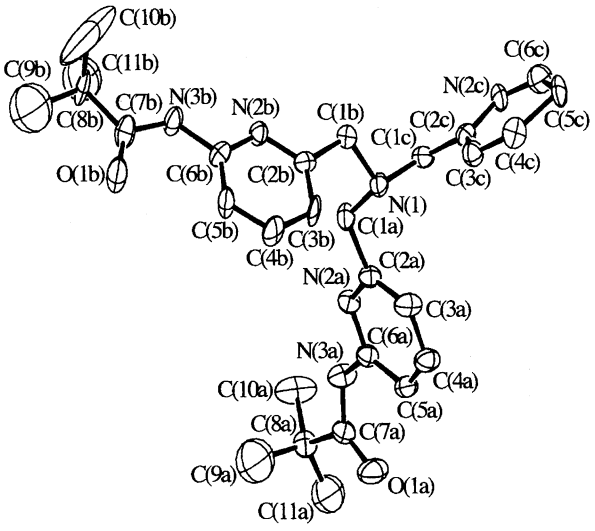

Fig. 1. ORTEP drawing of Hbppa with atomic labeling scheme.

actions of $[Cu(Hbppa)](ClO_4)_2$ with anions such as Cl^-, Br^-, I^-, N_3^-, OH^-, and CH_3COO^- at a 1 : 1 molar ratio in MeCN or MeOH are listed in Table 2. The complex solutions showed d–d transition bands in the range of 600—1000 nm and weak bands assignable to LMCT in the shorter wavelength region. Specifically, the complex with N_3^- exhibited the d–d bands characteristic of a trigonal-bipyramidal geometry.[21] The complex obtained from reaction of $[Cu(Hbppa)](ClO_4)_2$ with OH^- also was found to be trigonal-bipyramidal, although it was considered to be $[Cu(bppa)]ClO_4$ by judging from the elementary analyses. The complexes have weak absorption bands assignable to LMCT at 380—440 nm. Such weak LMCT bands are observed also in the Cu(II)–Htppa systems.[13d] On the other hand, the complexes with Cl^-, Br^-, I^-, and CH_3COO^- gave a spectral pattern typical of a square-pyramidal geometry.[21]

The frozen solution ESR spectra were also measured for these complexes (Table 3). Those of the complexes with N_3^- and CH_3COO^- exhibited the spectral pattern characteristic of a trigonal-bipyramidal geometry,[21] that of $[Cu(bppa)]ClO_4$ was also trigonal-bipyramidal, and those with Cl^-, Br^-, and I^- gave a spectral pattern typical of a square-pyramidal or square-planar geometry,[21] which agree well with those quessed from the electronic absorption spectra. These facts suggest that the Cu(II)–Hbppa complex can flexibly form a variety of structures depending on the secondary ligands and can accommodate bulky secondary ligands other than the Cu(II)–Htppa complex.[13d]

Structures of $[Cu(Hbppa)](ClO_4)_2$ and $[Cu(Hbppa)(N_3)]ClO_4 \cdot H_2O$. The crystal structures of $[Cu(Hbppa)](ClO_4)_2$ and $[Cu(Hbppa)(N_3)]ClO_4 \cdot H_2O$ demonstrate that the geometries around the Cu(II) ions were square-planar and a trigonal-bipyramidal geometries, respectively, as were concluded from the above-mentioned solution structures. The molecular structures of these complexes are depicted in Figs. 2 and 3, respectively, and their selected bond parameters are presented in Table 4. The Cu(II) ion in $[Cu(Hbppa)](ClO_4)_2$ was coordinated with a tertiary amine nitrogen (Cu–N(1) = 2.009(4) Å), two pyridine nitrogens (Cu–N(2a) = 1.957(4), Cu–N(2b) = 1.925(4) Å) and one pivalamido oxygen (Cu–O(1b) = 1.920(3) Å) of Hbppa in the equato-

Table 2. Electronic Absorption Spectral Data for Cu(II)–Hbppa Complexes

Complex/Solvent	LMCT (nm)/ε (M^{-1} cm^{-1})	d–d (nm)/ε (M^{-1} cm^{-1})
[Cu(Hbppa)]$(ClO_4)_2$/MeCN	—[b]	640 (sh,140), 734 (155), 950 (sh,90)
/MeOH	—[b]	602 (135)
$[Cu(Hbppa)Cl]^+$/MeCN	—[b]	700 (sh,138), 856 (219)
/MeOH	—[b]	700 (sh,125), 854 (172)
$[Cu(Hbppa)Br]^+$ [a]/MeCN	—[b]	700 (sh,180), 854 (237)
$[Cu(Hbppa)I]^+$ [a]/MeCN	530 (sh,120)	650 (sh,120), 850 (180)
[Cu(Hbppa)(N_3)]ClO_4/MeCN	380 (1170)	650 (252), 840 (256)
[Cu(bppa)]ClO_4/MeOH	430 (70)	629 (130), 815 (103)
[Cu(Hbppa)(CH_3COO)]ClO_4/MeCN	437 (51)	687 (sh,47), 788 (165)

a) Not isolated. b) Not observed.

Table 3. ESR Spectral Data for Cu(II)–Hbppa Complexes[a]

Complex/Solvent	ESR parameters			
[Cu(bppa)]$(ClO_4)_2$/MeCN	$g_{\parallel} = 2.21$	($A_{\parallel} = 186$ G),	$g_{\perp} = 2.01$	
[Cu(bppa)]$(ClO_4)_2$/MeOH	$g_{\parallel} = 2.22$	($A_{\parallel} = 191$ G),	$g_{\perp} = 2.06$	
$[Cu(bppa)Cl]^+$/MeOH	$g_{\parallel} = 2.22$	($A_{\parallel} = 186$ G),	$g_{\perp} = 2.06$	
$[Cu(bppa)Br]^+$ [b]/MeCN	$g_{\parallel} = 2.21$	($A_{\parallel} = 183$ G),	$g_{\perp} = 2.06$	
$[Cu(bppa)I]^+$ [b]/EtCN	$g_{\parallel} = 2.21$	($A_{\parallel} = 178$ G),	$g_{\perp} = 2.07$	
[Cu(bppa)(N_3^-)]ClO_4/EtCN	$g_{\perp} = 2.23$	($A_{\perp} = 116$ G),	$g_{\parallel} = 2.02$	($A_{\parallel} = 76$ G)
[Cu(bppa$^-$)]ClO_4/MeCN	$g_{\perp} = 2.21$	($A_{\perp} = 83$ G),	$g_{\parallel} = 2.01$	($A_{\parallel} = 117$ G)
[Cu(bppa)(CH_3COO^-)]ClO_4/MeCN	$g_{\perp} = 2.23$	($A_{\perp} = 106$ G),	$g_{\parallel} = 1.97$	($A_{\parallel} = 89$ G)

a) G denotes gauss. b) Not isolated.

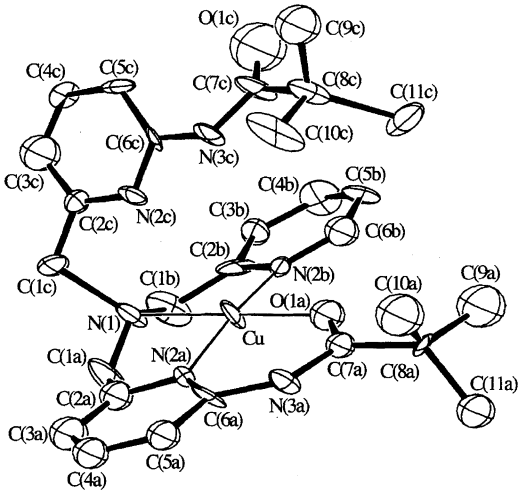

Fig. 2. ORTEP drawing of $[Cu(Hbppa)]^{2+}$ with atomic labeling scheme.

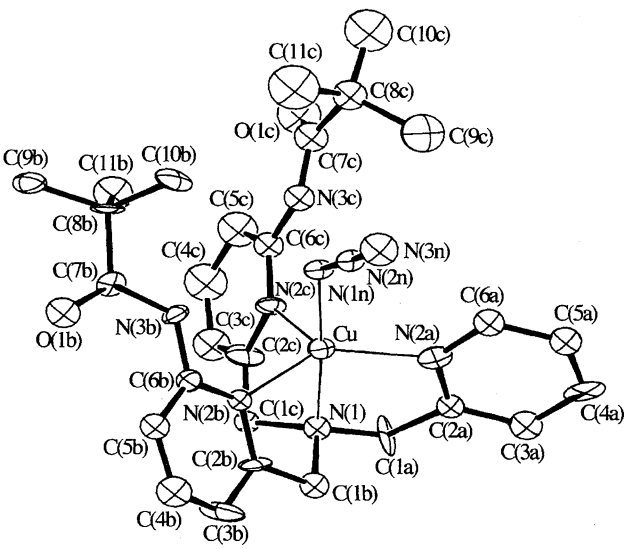

Fig. 3. ORTEP drawing of $[Cu(Hbppa)(N_3)]^+$ with atomic labeling scheme.

rial plane and the remaining pivalamide-substituted pyridyl group is apart from the central metal ion. The Cu(II) ion in the [Cu(Hbppa)(N_3)]ClO_4 was surrounded with three pyridine nitrogens of Hbppa (Cu–N(2a) = 2.056(7), Cu–N(2b) = 2.102(7), Cu–N(2c) = 2.217(7) Å) in the trigonal-plane and with a tertiary amine nitrogen (Cu–N(1) = 1.987(7) Å) and an azide ion (Cu–N(1n) = 1.937(7) Å) in the axial positions, just in the same way as $[Cu^{II}(Htppa)Cl]ClO_4$, $[Cu^{II}(Htppa)(OH)]$-ClO_4, $[Cu^{II}(Htppa)](ClO_4)_2 \cdot 2H_2O \cdot CH_3OH$, $[Cu^{II}(tppa)$-$(OH)] \cdot 2H_2O \cdot CH_3COCH_3$, and $[Cu^{II}(tppa)](BPh_4)$ reported previously.[13d] As have been pointed out in the Cu–Htppa complexes,[13a,13c,13d] the hydrogen bonds, N(1n)···N(3b) (2.94 Å) and N(1n)···N(3c) (2.97 Å), clearly contribute to the fixation of the azide ion. These findings from solution and solid state structures allow us to conclude that the Cu–Hbppa complex can from several geometries, such as square-planar, square-pyramidal, and trigonal-bipyramidal ones, and that it can incorporate one more bulky anion into its metal center than the metal center in the Cu–Htppa complex,[13d] indicating that the Cu–Hbppa system is liable to accommodate a substrate into its hydrophobic space.

Electrochemical Properties. The cyclic voltammo-

Table 4. Selected Bond Lengths (Å) and Angles (deg) for [Cu(Hbppa)]$(ClO_4)_2$, [Cu(Hbppa)(N_3)]$PF_6 \cdot H_2O$, and [Cu(Hbppa)(OH)]$ClO_4 \cdot H_2O$

[Cu(Hbppa)]$(ClO_4)_2$		[Cu(Hbppa)(N_3)]$ClO_4 \cdot H_2O$		[Cu(Hbppa)(OH)]$PF_6 \cdot H_2O$	
Cu–O(1b)	1.920(3)	Cu–N(1n)	1.937(7)	Cu–O(1h)	1.849(5)
Cu–N(1)	2.009(4)	Cu–N(1)	1.987(7)	Cu–N(1)	1.973(6)
Cu–N(2a)	1.957(4)	Cu–N(2a)	2.056(7)	Cu–N(2a)	2.086(6)
Cu–N(2b)	1.925(4)	Cu–N(2b)	2.102(7)	Cu–N(2b)	2.193(5)
		Cu–N(2c)	2.217(7)	Cu–N(2c)	2.166(6)
O(1b)–Cu–N(1)	177.3(2)	N(1n)–Cu–N(1)	175.8(3)	O(1h)–Cu–N(1)	177.4(3)
O(1b)–Cu–N(2a)	97.3(2)	N(1n)–Cu–N(2a)	100.6(3)	O(1h)–Cu–N(2a)	98.0(2)
O(1b)–Cu–N(2b)	92.0(2)	N(1n)–Cu–N(2b)	99.1(3)	O(1h)–Cu–N(2b)	101.1(2)
N(1)–Cu–N(2a)	85.3(2)	N(1n)–Cu–N(2c)	97.5(3)	O(1h)–Cu–N(2c)	96.0(2)
N(1)–Cu–N(2b)	85.5(2)	N(1)–Cu–N(2a)	83.2(3)	N(1)–Cu–N(2a)	83.8(3)
N(2a)–Cu–N(2b)	165.4(2)	N(1)–Cu–N(2b)	79.1(3)	N(1)–Cu–N(2b)	79.1(2)
		N(1)–Cu–N(2c)	79.7(3)	N(1)–Cu–N(2c)	81.5(3)
		N(2a)–Cu–N(2b)	136.8(3)	N(2a)–Cu–N(2b)	130.7(2)
		N(2a)–Cu–N(2c)	104.5(3)	N(2a)–Cu–N(2c)	108.9(2)
		N(2b)–Cu–N(2c)	110.6(3)	N(2b)–Cu–N(2c)	113.6(2)

grams of the complex [Cu(Hbppa)Cl]Cl were measured in several solvents under Ar (Table 5). All results revealed a quasi-reversible one-electron redox potential in the range of −0.056—+0.085 V vs. Ag/AgCl with a pair of cathodic and anodic waves of the Cu(II)/Cu(I) couple. The $E_{1/2}$ values obtained (+0.166—+0.307 V when converted to the NHE scale by the addition of +0.222 V[16]) are significantly lower than that of the previous [Cu(Htppa)Cl]ClO_4 complex (+0.447 V vs. NHE);[13d] on the other hand, they are higher than that [Cu(tmpa)Cl]PF_6 (tmpa = tris(2-pyridylmethyl)amine) (−0.39 V vs. NHE).[22] The order of the redox potentials of the complexes: tmpa < Hbppa < Htppa for the primary ligands, may be explained in terms of the electron densities on the central metal ions. The electron-withdrawing pivalamido group decreases the electron density on the metal ion and then increases the redox potential. The redox potential of the Cu–Hbppa complex established here lies between those of the Cu–tmpa[22] and Cu–Htppa complexes,[13d] which agrees well with the number of electron-withdrawing pivalamido groups. The redox potentials of this copper complex did not reveal any marked solvent-dependence in comparison with [Cu(Htppa)Cl]ClO_4.[13d]

Reaction of [Cu^{I}(Hbppa)]PF_6 with Dioxygen. Reaction of the [Cu^{I}(Hbppa)]PF_6 complex with dioxygen was performed in EtCN and MeOH, followed by electronic absorption and ESR spectra. The absorption spectra of the EtCN solution containing [Cu^{I}(Hbppa)]PF_6 at −78 °C exhibited a remarkable spectral change by bubbling of dioxygen into the solution, which was extremely slow. After 18 h, the spectral change completed with new and two well-separated d–d bands at 665 nm ($\varepsilon = 162$ M^{-1} cm^{-1}) and 837 nm ($\varepsilon = 305$ M^{-1} cm^{-1}), and an absorption band at 375 nm ($\varepsilon = 641$ M^{-1} cm^{-1}) assignable to LMCT. The spectral pattern of the d–d bands was typical of the Cu(II) complex with a trigonal-bipyramidal geometry,[13d] and the LMCT band observed here lies in the intermediate region of the bands reported previously, [Cu(tmpa)(O_2)]$^+$ (410 nm, $\varepsilon = 4000$ M^{-1} cm^{-1}),[22] [Cu(bqpa)(O_2)]$^+$ (378 nm, $\varepsilon = 8200$ M^{-1} cm^{-1}) and [Cu(Htppa)(O_2)]$^+$ (315 nm, ε = ca. 4000 M^{-1} cm^{-1})[13a,13d] (tmpa = tris(2-pyridylmethyl)amine, bqpa = *N*-(2-pyridylmethyl)bis(2-quinolylmethyl)amine). Such a result may be explained in terms of the electronic characters of these ligands. Since the Hbppa and Htppa ligands have electron-withdrawing substituent groups, as compared with the tmpa and bqpa ligands, the bonds between the pyridine nitrogens and the copper atom are weakened and the binding of dioxygen to the metal atom is strengthened. The Hbppa ligand, which features one fewer pivalamido group than Htppa, may weaken the binding of dioxygen to Cu(II) than Htppa, which results in the longer wavelength shift of the LMCT band. The small ε value in LMCT may be explained as due to the distortion of orbital symmetry between the metal and dioxygen. Such spectral changes as described above were not observed for the Cu(I)–Htppa system in MeCN or EtCN.[13d] The ESR spectrum of the O_2 adduct of [Cu(Hbppa)]$^+$ in EtCN was silent, suggesting that the [Cu(Hbppa)]$^+$ complex reacts with dioxygen to generate [Cu(Hbppa)(O_2^-)]$^+$ species antiferromagnetically coupled.

On the other hand, the reaction with dioxygen in MeOH solution quickly proceeded and gave the d–d bands at 640 nm ($\varepsilon = 183$ M^{-1} cm^{-1}) and 828 nm ($\varepsilon = 289$ M^{-1} cm^{-1}) and the LMCT band at 387 nm ($\varepsilon = 843$ M^{-1} cm^{-1}) (Fig. 4). The LMCT band, however, immediately decreased in absorbance, although the d–d band positions did not show any remarkable changes. The final spectrum exhibited absorption peaks at 634 nm ($\varepsilon = 178$ M^{-1} cm^{-1}), 839 nm ($\varepsilon = 250$

Table 5. Cyclic Voltammetry Data for [Cu(Hbppa)Cl]Cl at Room Temperature

Solvent	$E_{1/2}$[a]/V	ΔE_p/V	i_{pa}/i_{pc}
THF	+0.085	0.170	0.74
CH_2Cl_2	+0.053	0.105	0.97
CH_3CN	−0.048	0.064	0.96
CH_3OH	−0.056	0.127	0.98

a) $E_{1/2} = (E_{pa} + E_{pc})/2$.

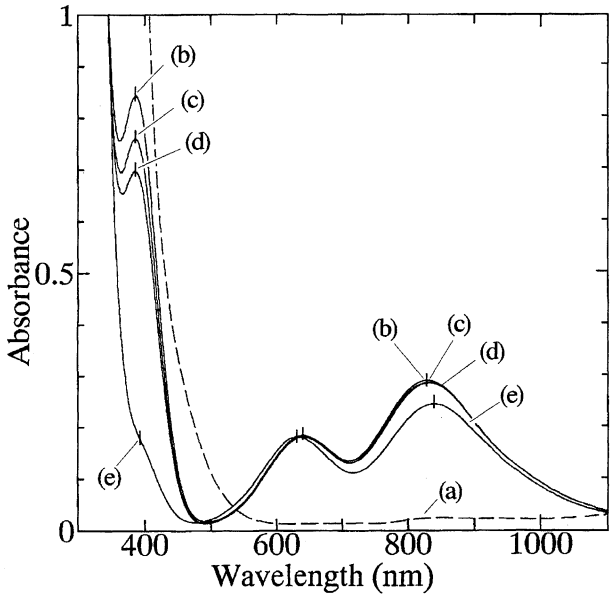

Fig. 4. Low-temperature electronic absorption spectra for the oxygenation reaction of $[Cu^{I}(Hbppa)]PF_6$ with dioxygen in MeOH at −78 °C. (a) $[Cu^{I}(Hbppa)]PF_6$; after the reaction with dioxygen (b) 10 min; (c) 1 h; (d) 3 h; (e) final.

$M^{-1}\,cm^{-1}$) and 400 nm ($\varepsilon = 150\ M^{-1}\,cm^{-1}$); this spectral pattern is very similar to that observed when the temperature of the complex solution was increased up to room temperature. This finding indicates that the O_2 adduct was formed once in MeOH, but it was decomposed or replaced by methoxide ion. The ESR spectrum of the complex in MeOH, in contrast with that in EtCN, showed weak signals at first, but the intensity of them gradually increased. The ESR parameters at the end point of the reaction are $g_{\perp} = 2.21$ ($A_{\perp} = 69$ gauss) and $g_{\parallel} = 2.01$ ($A_{\parallel} = 94$ gauss), which is a pattern typical to a trigonal-bipyramidal Cu(II) species. The behavior of this ESR spectral change is very similar to that of the electronic absorption spectral one. These results suggest that superoxide is generated in these systems. Standing the solution of this complex at room temperature gave a green single crystal suitable for X-ray analysis, whose crystal structure, as shown in Table 4, revealed that it was $[Cu(Hbppa)(OH)]PF_6 \cdot H_2O$ of a trigonal-bipyramidal geometry (Fig. 5) with three pyridine nitrogens of Hbppa (Cu–N(2a)=2.086(6), Cu–N(2b)=2.193(5), Cu–N(2c)=2.166(6) Å) in the trigonal-plane and with a tertiary amine nitrogen (Cu–N(1)=1.973(6) Å) and hydroxide ion (Cu–O(1h) = 1.849(5) Å) in the axial positions. The formation of a hydroxide complex was also noticed in the Cu–Htppa system,[13c] although the origin of the hydrogen atom is not clear at present.

Reaction of the Cu(I)–Hbppa–Sodium Benzoylformate System with Dioxygen. The evolution of superoxide from the Cu(I)–Hbppa–O_2 system was suggested in the preceeding section. That allows us to expect the oxidative cleavage reaction of α-keto acid which is a characteristic reaction of superoxide.[23–25] Here the reaction in the Cu(I)–Hbppa–O_2–sodium benzoylformate system was tested. For comparison, the reaction was also performed on the copper complexes of Htppa, bpqa and tnpa as well as for Hbppa (Chart 1). The reactions were carried out by addition of sodium benzoylformate to a DMF solution containing $[Cu(MeCN)_4]ClO_4$ and the tripodal tetradentate ligands (Hbppa, Htppa, tnpa, bpqa) under an Ar atmosphere at room temperature. After stirring the reaction mixture for ca. 15 min, the resultant yellowish solution was cooled at −78 °C and was bubbled with O_2 gas. After the temperature of the reaction solution was raised to room temperature and the solution was stirred for 4 h, CO_2 gas was detected by GC analysis in the reaction vessel, suggesting that the decarboxylation of benzoylformate proceeded. The yield of the decarboxylated product, benzoic acid, was determined by HPLC analysis. The yields of benzoic acid after the reactions for 4 h increased in the order of: bpqa (13%) < Htppa (19%) < tnpa (30%) < Hbppa (38%) for the primary ligands. There were no compounds other than the product, benzoic acid, and the starting material, benzoylformate. This reaction did not proceed at all in the absence of O_2 and/or Cu(I) ion. Previously, the oxidative cleavage reaction of α-keto acids with potassium superoxide was reported by Valentine et al.; it was carried out using a 4 : 1 ratio of KO_2 to α-keto acid for 24 h and the yields of the products were in the range of 42—93%.[23] The yield of the product observed in this Cu(I)–Hbppa–α-keto acid–O_2 system is comparable to those reported by Valentine et al.[23] The reactivity order mentioned above may be explained as follows: The Cu–bpqa and –Htppa complexes hinder the approach of the substrate to the active center sterically, whereas the Cu–tnpa and –Hbppa complexes give little steric effect. The highest yield of benzoic acid observed in the Cu–Hbppa system may suggest the presence of an appropriate space for approaching of the substrate to the active center.

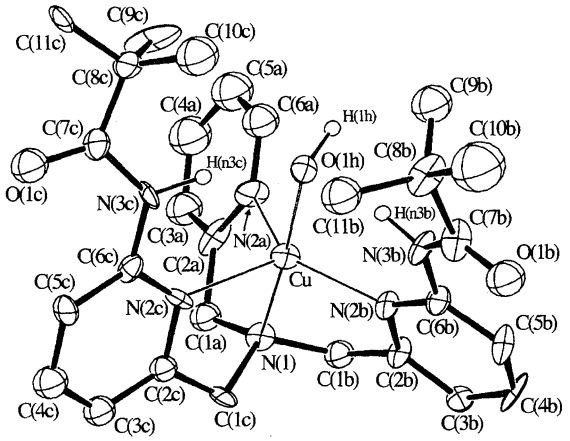

Fig. 5. ORTEP drawing of [Cu(Hbppa)(OH)] with atomic labeling scheme.

We are grateful to the Institute for Molecular Science for the use of the JEOL Lambda-500 NMR spectrometer and the Shimadzu Kratos Concept I S mass spectrometer. This research was supported in part by a Grant-in-Aid for Scientific Research from the Ministry of Education, Science, Sports and Culture (M. H., K. J., and H. M.).

References

1) M. Momenteau and C. A. Reed, *Chem. Rev.*, **94**, 659 (1994).
2) J. H. Dawson, *Science*, **240**, 433 (1988).
3) A. L. Feig and S. J. Lippard, *Chem. Rev.*, **94**, 759 (1994).
4) L. Que, Jr., "Bioinorganic Catalysis," ed by J. Reedijk, Marcel Dekker, Inc., New York (1993), p. 347.
5) S. Fox and K. D. Karlin, "Active Oxygen in Biochemistry," ed by J. S. Valentine, C. S. Foote, A. Greenberg, and J. F. Liebman, Blackie Academic & Professional, Chapman & Hall, Glasgow (1995), p. 188.
6) N. Kitajima and Y. Moro-oka, *Chem. Rev.*, **94**, 737 (1994).
7) "Bioinorganic Chemistry of Copper," ed by K. D. Karlin and Z. Tyeklar, Chapman & Hall, New York (1993).
8) K. D. Karlin, Z. Tyeklar, and A. D. Zuberbuhler, "Bioinorganic Chemistry," ed by J. Reedijk, Marcel Dekker, Inc., New York (1993), p. 261.
9) E. I. Solomon, F. Tuczek, D. E. Root, and C. A. Brown, *Chem. Rev.*, **94**, 827 (1994).
10) E. I. Solomon and M. D. Lowery, *Science*, **259**, 1575 (1993).
11) J. P. Klinman, *Chem. Rev.*, **96**, 2541 (1996).
12) "Mechanistic Bioinorganic Chemistry," ed by H. H. Thorp and V. L. Pecoraro, American Chemical Society, Washington, D.C. (1995).
13) a) M. Harata, K. Jitsukawa, H. Masuda, and H. Einaga, *J. Am. Chem. Soc.*, **116**, 10817 (1994); b) M. Harata, K. Jitsukawa, H. Masuda, and H. Einaga, *Chem. Lett.*, **1995**, 61; c) M. Harata, K. Jitsukawa, H. Masuda, and H. Einaga, *Chem. Lett.*, **1996**, 813; d) M. Harata, K. Jitsukawa, H. Masuda, and H. Einaga, *Bull. Chem. Soc. Jpn.*, **71**, 637 (1998).
14) M. Harata, K. Jitsukawa, H. Masuda, and H. Einaga, *J. Coord. Chem.*, in press (1998).
15) A. Wada, M. Harata, K. Hasegawa, K. Jitsukawa, H. Masuda, M. Mukai, T. Kitagawa, and H. Einaga, *Angew. Chem., Int. Ed. Engl.*, in press (1998).
16) J. O'M. Bockris and A. K. N. Reddy, "Modern Electrochemistry," Plenum Press, New York (1970).
17) K. Hasegawa, M. Harata, K. Jitsukawa, H. Masuda, and H. Einaga, submitted for publication.
18) A. Wada, M. Harata, K. Jitsukawa, H. Masuda, and H. Einaga, submitted for publication.
19) "International Tables for X-Ray Crystallography," Kynoch Press, Birmingham, U.K. (1974), Vol. IV.
20) Enraf-Nonius, "MolEN, An Interactive Structure Solution Procedure," Enraf–Nonius, Delft, The Netherlands (1990).
21) B. J. Hathaway, "Comprehensive Coordination Chemistry," ed by G. Wilkinson, Pergamon Press, Oxford (1987), Vol. 5, p. 533.
22) a) K. D. Karlin, N. Wei, B. Jung, S. Kaderli, P. Niklaus, and A. D. Zuberbuhler, *J. Am. Chem. Soc.*, **115**, 9506 (1993); b) N. Wei, N. N. Murthy, Z. Tyeklar, and K. D. Karlin, *Inorg. Chem.*, **33**, 1177 (1994); c) N. Wei, N. N. Murthy, Q. Chen, J. Zubieta, and K. D. Karlin, *Inorg. Chem.*, **33**, 1953 (1994).
23) J. S. Filippo, Jr., C-I. Chern, and J. S. Valentine, *J. Org. Chem.*, **41**, 1077 (1976).
24) Y.-M. Chiou and L. Que, Jr., *J. Am. Chem. Soc.*, **117**, 3999 (1995).
25) E. H. Ha, R. Y. N. Ho, J. F. Kisiel, and J. S. Valentine, *Inorg. Chem.*, **34**, 2265 (1995).
26) P. Tomasik and R. Zalewski, *Chem. Zvesti*, **31**, 246 (1977).